UV−vis Spectroscopic Properties of nC(60) Produced via Extended Mixing

ARTICLE *in* ENVIRONMENTAL SCIENCE & TECHNOLOGY · DECEMBER 2011

Impact Factor: 5.33 · DOI: 10.1021/es201229a · Source: PubMed

2 AUTHORS:

Xiaojun Chang
Virginia Polytechnic Institute and State Univ…
9 PUBLICATIONS **93** CITATIONS
SEE PROFILE

Peter Vikesland
Virginia Polytechnic Institute and State Univ…
90 PUBLICATIONS **2,001** CITATIONS
SEE PROFILE

Environmental Science & Technology

ARTICLE

pubs.acs.org/est

UV−vis Spectroscopic Properties of nC_{60} Produced via Extended Mixing

Xiaojun Chang[†,‡] and Peter J. Vikesland[*,†,‡]

[†]Department of Civil and Environmental Engineering, and Institute for Critical Technology and Applied Science (ICTAS), Virginia Tech, Blacksburg, Virginia, United States

[‡]NSF-EPA Center for the Environmental Implications of Nanotechnology (CEINT)

Supporting Information

ABSTRACT: Colloidally stable C_{60} suspensions produced via extended mixing in water (aq/nC_{60}) are highly heterogeneous with respect to particle size and morphology. Ultraviolet−visible (UV−vis) absorption spectra of aq/nC_{60} are often used as a supplemental tool to dynamic light scattering (DLS), transmission electron microscopy (TEM), and other analytical methods to characterize aq/nC_{60}. In the present study, the UV−vis spectra provide information about the average particle size and the interactions between C_{60} and water. We report that the decrease in relative absorption in the 240−290 nm range is a function of magnetic stirring time, that the average size (Z_{ave}) of an aq/nC_{60} suspension determines the position of absorbance maximum of its 360 nm band, and that the methods used to prepare and fractionate nC_{60} affect the extent of the blue shift in this band that occurs due to a decrease in Z_{ave}. We also confirm that the broad absorption band in the 400−600 nm region is a result of C_{60} aggregation.

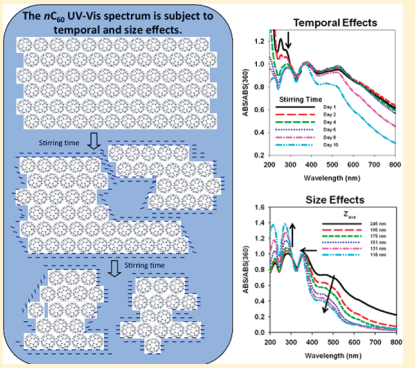

INTRODUCTION

The ultraviolet−visible (UV−vis) spectra of fullerene C_{60} in the gas phase and organic solvents[1,2] have been extensively studied since the discovery of C_{60} in 1985. In the gas phase, C_{60} exhibits sharp absorption bands that broaden when C_{60} is dispersed in liquids or solutions due to solvation effects as well as the increased number of interactions between neighboring C_{60} molecules.[3,4] Accordingly, the absorption spectrum of C_{60} in a solution is highly dependent upon the properties of the solvent.[5] Fullerene C_{60} has appreciable solubility in aromatic and nonpolar solvents (e.g., 2150 mg/L in toluene, 1440 mg/L in benzene, and 40 mg/L in *n*-hexane[6]), but is only sparingly soluble in polar solvents (e.g., 35 μg/L in methanol and 800 μg/L in ethanol[7]). For true C_{60} solutions, in which C_{60} is dispersed as individual molecules, the shape, the position of absorption maximum, and the relative absorbance of each band in the UV−vis spectrum change with solvent identity.[2] Previous studies[2,5,8] have reported the effect of solvent properties (e.g., polarizability parameter, polarity parameter, molecular volume, Hildebrand solubility, etc.) on the spectra of fullerene solutions.

Although it has extremely low solubility in water, C_{60} forms colloidally stable aqueous suspensions consisting of nanoscale particles (nC_{60})[9−12] instead of a true solution of dispersed individual molecules. As a result, nC_{60} suspensions exhibit UV−vis spectra that differ from those of true C_{60} solutions in organic solvents. Although the spectra of nC_{60} reported in the literature are generally similar, they often subtly differ from one another depending upon the preparation methods (solvent exchange, sonication, or extended mixing) and solution chemistries employed.[9,11,13,14] Compared with the well-characterized spectra of C_{60} in organic solvents, the spectral properties of nC_{60} suspensions are not well understood even though UV−vis spectra for nC_{60} in the presence of natural organic matter and other solutes are commonly presented to illustrate nC_{60} production.[15−17] As documented herein, interpretation of UV−vis spectra can be a powerful tool to investigate the properties of nC_{60} suspensions.

Both transmission electron microscopy (TEM) and dynamic light scattering (DLS) are commonly used to characterize the size and structure of nC_{60} suspensions; however, TEM requires the use of dried samples and DLS is inherently challenged by highly heterogeneous suspensions such as nC_{60}. The drying process may induce artifacts that reduce the reliability of the collected images,[18] and the hydrodynamic diameter (Z_{ave}) determined by DLS is an average of all peaks in the particle size distribution for a highly polydisperse suspension such as nC_{60}.[12] As a result, two nC_{60} samples with similar Z_{ave} values may have very different structural characteristics due to their inherent heterogeneity. UV−vis spectroscopy is an in situ technique that measures the spectroscopic properties of suspensions and provides direct information that can provide insights into the interactions between C_{60} and solution constituents.

Recently Kato et al.[19] and Deguchi et al.[20] provided the first attempts to systematically evaluate the UV−vis spectra of nC_{60}

Received: April 11, 2011
Accepted: October 19, 2011
Revised: October 12, 2011
Published: October 19, 2011

solutions produced by THF solvent exchange and sonication/surfactant stabilization, respectively. Each of these studies indicates that the spectral properties of nC_{60} suspensions are a function of the nC_{60} particle size with the measured absorption bands blue-shifting as the particle size decreases. Both Kato et al.[19] and Deguchi et al.[20] hypothesized that these changes in the absorption properties reflect an increase in the number of interactions between water molecules and the C_{60} surface that occurs concomitant with a decrease in particle size. Unfortunately because their nC_{60} suspensions were produced either by solvent exchange or sonication/surfactant stabilization it is not clear how readily their conclusions translate to aqueous systems devoid of residual solvents (e.g., THF) or surfactants (e.g., sodium dodecylsulfate). In the present study, we provide the first detailed analysis of the UV−vis spectroscopic properties of nC_{60} produced via extended mixing in water in the absence of any organic solvents or surfactants.

EXPERIMENTAL SECTION

Materials. Sublimed C_{60} (>99.9% pure) was purchased from Materials Electronics Research Corporation (Tucson, AZ). Reagent-grade toluene and ACS-grade *n*-hexane were purchased from Sigma Aldrich and Mallinckrodt Chemical, respectively. All glassware was washed with aqua regia and rinsed thoroughly before use. All water (>18.2 MΩ-cm) used in this study was obtained from a Barnstead NANOpure water purification system.

Sample Preparation. C_{60}−*n*-hexane and C_{60}−toluene solutions were prepared by directly dissolving as-purchased fullerene C_{60} powder in the solvents. Stable aqueous C_{60} colloidal suspensions (aq/nC_{60}) were prepared via extended mixing.[12,21,22] As-purchased fullerene C_{60} was pulverized (amplitude 0.5 mm for 20 min) in a Fritsch pulverizette 0 ball mill to reduce its irregularity and initial size. The resulting powder was sieved through a 63-μm metal sieve and stored in the dark. ICP-MS analysis of the pulverized material did not indicate the presence of any residual metals within the resultant C_{60} powder. Pulverized powder was added to nanopure water at a concentration of 400 mg C_{60}/L. The mixture was magnetically stirred at 500 rpm in the dark at room temperature. To characterize changes in aq/nC_{60} properties over time, sample aliquots of 2.5 mL were removed periodically and settled for 24 h before 2.0-mL samples of supernatant were characterized. The supernatant of an aq/nC_{60} suspension prepared using a 30-day stirring time and a 15-day settling period was transferred to a clean glass vial and stored in the dark as stock aq/nC_{60}.

Particle Size Discrimination by Centrifugation. Aliquots (5 mL) of stock aq/nC_{60} were centrifuged at 7000 rpm for time periods of 1−40 min in a Beckman J2-HS centrifuge and 3.5 mL of the supernatant was transferred to a test tube for characterization. In a second experiment, stock aq/nC_{60} suspension was diluted by nanopure water at a dilution ratio (= final suspension volume/stock aq/nC_{60} volume) of 4:1. The resulting suspension was then subjected to the same centrifugation and characterization procedures.

***n*C_{60} Characterization.** The average particle size (represented by hydrodynamic diameter, Z_{ave}, and polydispersity index, PDI) and the average surface charge (represented by the electrophoretic mobility, EM) of the aq/nC_{60} suspensions were measured using a Malvern NanoZS dynamic light scattering (DLS) instrument and a disposable folded capillary cell. Details regarding the DLS measurements are found elsewhere.[21] UV−vis absorption spectra of aq/nC_{60} were recorded using a Cary 5000 UV−vis-NIR spectrophotometer at room temperature using a quartz cuvette with a path length of 1 cm. The cuvette was filled with 2.5 mL of aq/nC_{60} solution and scanned over a range of 200−800 nm at a bandwidth of 1 nm using double beam mode. Each of the spectra of aq/nC_{60} were obtained using a nanopure water background. Absorption spectra of C_{60} in toluene and *n*-hexane were measured using the same spectrophotometer, with background corrections of toluene and *n*-hexane, respectively.

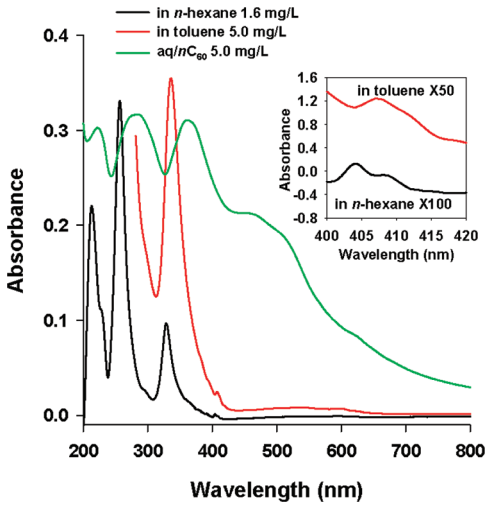

Figure 1. UV−vis spectra of C_{60} in *n*-hexane, toluene, and aq/nC_{60}.

RESULTS AND DISCUSSION

A true solution of C_{60} in *n*-hexane exhibits a characteristic spike in the UV−vis spectrum at 404 nm as well as three major absorption bands at 211, 257, and 328 nm (Figure 1). The UV−vis spectrum of a C_{60}−toluene solution shows a similar spike at 407 nm and an additional absorption band at 336 nm. The C_{60}−toluene solution does not exhibit absorption bands at lower wavelengths (<280 nm) because of the intrinsic absorption of the toluene aromatic ring. Compared with the spectra of well-dispersed C_{60} in organic solvents, aq/nC_{60} exhibits three absorption peaks at 221, 288, and 369 nm. As previously described,[11,23−25] these absorption bands are red-shifted and broader than the corresponding absorption bands in either toluene or *n*-hexane. These differences occur as a result of the extended electronic interactions possible within the crystalline lattice of nC_{60} as well as light scattering by the nC_{60} nanoparticles.

In aq/nC_{60} the spike in the 400−410 nm region, which is a vibronic signal (reflecting changes in vibrational energy under irradiation[3]) observed in the C_{60}-organic solutions, disappears while a continuous absorption band is observed in the 400−600 nm region. The vibronic signal results from coupling of the weak symmetry-allowed 1^1T_{1u}-1^1A_g electronic transition with intramolecular vibrational features.[2] When C_{60} is present in particle form the molecular orbitals arising from π-orbital interactions between fullerene molecules become broader. These intermolecular effects perturb the 1^1T_{1u}-1^1A_g transition to such a degree that it is no longer visible for nC_{60}.[26] The appearance of the continuous absorption band between 400 and 600 nm has been previously assigned to the parity forbidden HOMO−LUMO transition ($h_u - t_{1u}$) in C_{60} thin films[27] or to the formation of weak donor−acceptor complexes between C_{60} and water.[28]

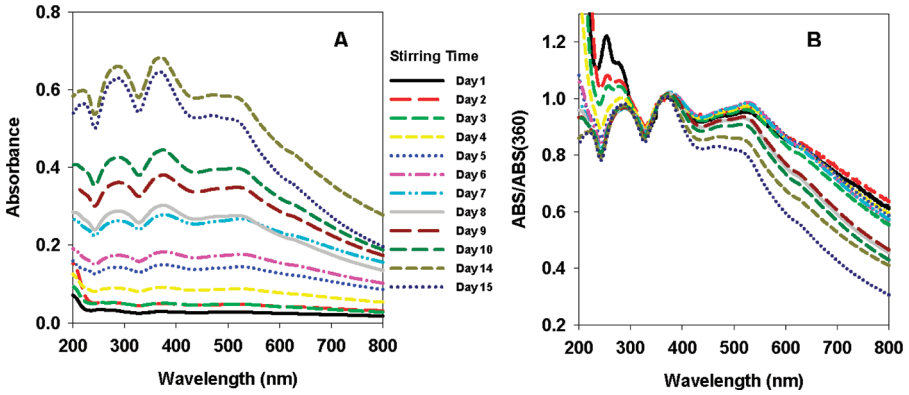

Figure 2. (A) UV−vis spectra and (B) normalized spectra of aq/nC$_{60}$ produced by extended mixing.

For the first time that we are aware, the origins of this band are fully assessed for aq/nC$_{60}$ in the sections that follow.

Our negatively charged aq/nC$_{60}$ nanoparticles were obtained by magnetic stirring. The surface charge (represented by the measured electrophoretic mobility) of aq/nC$_{60}$ is stable during the extended mixing period, while the average particle size (represented by hydrodynamic diameter, Z_{ave}) decreases from >550 nm at the beginning of the stirring period to 270 nm after 15 days (Figure S1A). Simultaneous to the decrease in Z_{ave} is a reduction in solution polydispersity (Figure S1B). During the extended mixing period, the absorbance of the aq/nC$_{60}$ suspensions increases with stirring time (Figure 2A). This increase in absorption reflects the increase in C$_{60}$ concentration that occurs during mixing;[29] however, there are also subtle changes in the absorption spectra that occur over the mixing period. Figure 2B illustrates normalized absorption spectra produced by dividing the absorbance at each wavelength by the measured absorbance at 360 nm [ABS(360)]. This normalization scheme accounts for the change in absorbance due to the increase in the nC$_{60}$ concentration over time. As shown, there are readily discernible changes in the normalized spectra over time: (1) the spectra in the 240−290 nm region exhibit a general decline in relative intensity; (2) the peak in the 360 nm region shifts to shorter wavelengths; and (3) the relative intensity of the 400−600 nm absorption band decreases. In the sections that follow we systematically examine these changes in the spectra.

Changes in the 240−290 nm Region. The collected spectra in the 240−290 nm region are time-dependent (Figure S2A). After one day of stirring, the position of absorption maximum (λ_{max}) in this region was at 255 nm with a shoulder band at ≈280 nm. The relative absorbances of these peaks change over time. On days 2 and 3, there were two peaks (at 255 and 277 nm) in the normalized spectra. As stirring time increased, however, the 255 nm peak shrank to become a shoulder of the peak at 284 nm by day 4. After day 4 the peak at 255 nm had completely disappeared and λ_{max} in this region was stable at 288 nm (Figure 2B).

Leach et al.[1] have assigned the absorption bands of the spectra of C$_{60}$−n-hexane solutions to their corresponding electronic and vibrational transitions. In n-hexane, the peak at 257 nm is assigned to the allowed 6^1T_{1u}-1^1A_g transition and the absorption peak in the 285−305 nm region corresponds to the allowed 4^1T_{1u}-1^1A_g and 5^1T_{1u}-1^1A_g transitions. These transitions can be assigned to bands with slightly different λ_{max} values in other organic solvents.[5] Unfortunately, no similar work has been done in aqueous nC$_{60}$ suspensions to date. Although we do not know the exact origins of these absorption bands and the reason(s) for their spectral variation over time, it is reasonable to assign the bands at 255 and 288 nm to different electronic transitions. The temporal change in the relative intensities of these bands indicates that the interaction between C$_{60}$ and water progressively alters the spectroscopic properties of aq/nC$_{60}$. To our knowledge, no previous studies have documented these progressive changes in the relative intensity of these spectral bands. These changes perhaps reflect the development of hydrophilic groups at the nC$_{60}$ surface that have previously been detected by FTIR and ^{13}C NMR.[30−32] However, due to the extreme heterogeneity and polydispersity of the aq/nC$_{60}$ suspensions such a hypothesis requires additional testing.

Changes in the 360 nm Absorption Band. The position of absorption maximum of the ≈360 nm band (λ_{max}(360)) decreased from 378 to 369 nm between day 5 and day 15 (Figure S2B; Note: (1) the nC$_{60}$ concentrations prior to day 5 were too low to determine exact λ_{max}(360) values and (2) as discussed in the following sections, λ_{max} depends upon the average particle size. We note that although the wavelength range noted here is >360 nm, we use the term "360 nm band" to define this particular band later in the paper and use it here for consistency). As discussed *vide infra* this blue shift is both the result of the progressive change in the interactions between aq/nC$_{60}$ and water and of the decrease in the size of the nC$_{60}$ particles that occurs over time due to mixing (Z_{ave} = 390 nm on day 5 and Z_{ave} = 272 nm on day 15).

A centrifugation experiment was conducted to fractionate the aq/nC$_{60}$ suspensions to investigate whether mixing mediated changes in particle size were responsible for the blue shift of the 360 nm absorption band. Aq/nC$_{60}$ suspensions subjected to differential centrifugation periods had similar surface charges (≈3.0×10^{-8} m^2/V-s, Figure S3), but their average particle sizes decreased from 245 to 114 nm as the centrifugation time increased from 0 to 40 min. Importantly, solution polydispersity decreased following a 1-min centrifugation time and was then relatively constant for centrifugation times up to 20 min; centrifugation times longer than 20 min led to an increase in polydispersity (Figure S3B). The variability in the polydispersity as a function of centrifugation time follows a pattern that differs considerably from that observed for both the hydrodynamic diameter and the shift in the nC$_{60}$ absorption bands and thus the strong correlation between Z_{ave} and the 360-nm and 275-nm absorption bands cannot be due to changes in polydispersity.

Over the centrifugation period the absorbance at a fixed wavelength of 360 nm decreased from 1.52 to 0.04 (Figure S4).

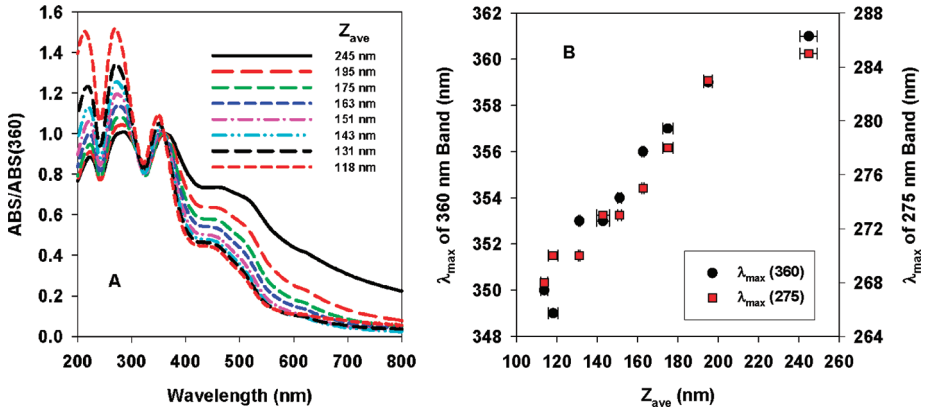

Figure 3. (A) Normalized UV−vis spectra of centrifuged aq/nC$_{60}$ and (B) λ_{max}(360) and λ_{max}(275) as a function of Z_{ave} (the Z_{ave} value represented in this figure is the average of three measurements and the error bar represents the standard deviation of three measurements).

This decrease in absorbance is the result of the declining total C$_{60}$ concentration as a result of centrifugation. Normalized spectra (Figure 3A), obtained by dividing the absorbance at each wavelength by its ABS(360), show that two major absorption bands shift to shorter wavelengths with a decrease in particle size. λ_{max}(360) and λ_{max}(275) decrease from 361 to 350 nm and from 285 to 268 nm, respectively (Figure 3B). To confirm this result and test the reproducibility of the relationship between λ_{max} and Z_{ave}, the centrifugation experiment was repeated, but using a diluted aq/nC$_{60}$ suspension (as described in the Experimental Section). The lack of any measurable difference between the results of the centrifuged diluted aq/nC$_{60}$ and the centrifuged stock aq/nC$_{60}$ suspensions (Figure S5) indicates that the relationship between λ_{max} and Z_{ave} is not concentration dependent.

A comparison of the blue shift of the 360 nm absorption band observed herein and that reported elsewhere[19,20] is shown in Figure 4A. The three curves shown are regression lines indicating the relationship between λ_{max} and Z_{ave} obtained in the present study and those of Deguchi et al.[20] and Kato et al.[19] These relationships are expressed by eqs 1, 2, and 3, respectively.

$$\lambda_{max}(360) = 0.087\ Z_{ave} + 340.1\ \text{nm} \quad (R^2 = 0.9074) \tag{1}$$

$$\lambda_{max}(360) = (0.065 \pm 0.009)\ Z_{ave} + (337.1 \pm 1.4)\ \text{nm} \tag{2}$$

$$\lambda_{max}(360) = 0.1429\ Z_{ave} + 325.7\ \text{nm} \tag{3}$$

The slope of the regression line indicates the extent of the blue shift that occurs for a given decrease in average particle size. The slopes from Deguchi et al. and our study are similar, yet smaller than that from Kato et al. The different slopes may reflect the different methods used to both produce and size-fractionate the nC$_{60}$ suspensions. In our studies, aq/nC$_{60}$ was produced by extended mixing in water, whereas Deguchi et al. produced nC$_{60}$ in the presence of surfactants and Kato et al. used THF/nC$_{60}$ in their studies. Furthermore, centrifugation and centrifugation/filtration were used in our experiments and the Deguchi et al.[20] study, respectively, while Kato et al.[19] employed the asymmetrical flow field flow fractionation (AF4) technique. Centrifugation and filtration selectively remove the largest particles from a suspension and thus only slightly reduce the polydispersity of a highly heterogeneous suspension (Figure S3b). In contrast, AF4 is known to produce suspensions with narrow particle size distributions.[33] As a result, size-fractionated nC$_{60}$ obtained by AF4 is expected to be less polydisperse than that obtained via centrifugation. For two suspensions with similar Z_{ave} values, the more polydisperse one will generally have a greater amount of large particles. The presence of these large particles would decrease the extent of the blue shift and alter the observed slope.

Absorption spectra of C$_{60}$ in organic solvents, micelles, and colloidal liposome solutions have been recorded at room temperature.[2,5,8,34] In these solvents, fullerene C$_{60}$ is primarily dispersed as individual molecules. Across this set of solvents there is a red shift of the 330-nm band that generally correlates with an increase in the solvent polarizability parameter (Figure 4B). The solvent polarizability parameter is derived from the Lorentz−Lorenz relation: $\phi(n^2) = (n^2 - 1)/(n^2 + 2)$, where n is the refractive index of the solvent. This red shift corresponds to a decrease in the electrostatic work required to produce the solute transition dipole in the dielectric medium in contact with each C$_{60}$ molecule,[35] thus indicating that the position of this absorption band provides information about the interaction between fullerene and the solvent molecules. For instance, the large red shift observed in aromatic solvents (λ_{max} = 335.0 and 335.5 nm for C$_{60}$ in benzene and toluene, respectively[2]) has been attributed to complex formation between C$_{60}$ and aromatic solvent molecules through $\pi-\pi$ interactions.[36] Using data from the literature that is summarized in Figure 4B we obtained the following regression relating solvent polarizability to λ_{max}(360):

$$\lambda_{max}(360) = (84.18 \pm 25.68)\ \phi(n^2) + (307.84 \pm 6.4) \tag{4}$$

We note that the large variability in the data presented in Figure 4B is reflected in the relatively large error in the slope for this regression. Even accounting for the wide degree of variability in the data it is nonetheless apparent that a decrease in the polarizability parameter generally correlates with a red-shift in the absorption spectrum. For water the polarizability parameter (n = 1.33) is 0.204. Using this value in eq 4, the λ_{max}(360) of a "hypothetical" aqueous molecular C$_{60}$ solution is predicted to be 325 ± 6.4 nm.

A previous study[37] reported that λ_{max}(360) for a series of C$_{60}$−SDBS solutions decreased from 344 to 330 nm as the concentration of SDBS increased from 0.5 to 50 g/L. Across this

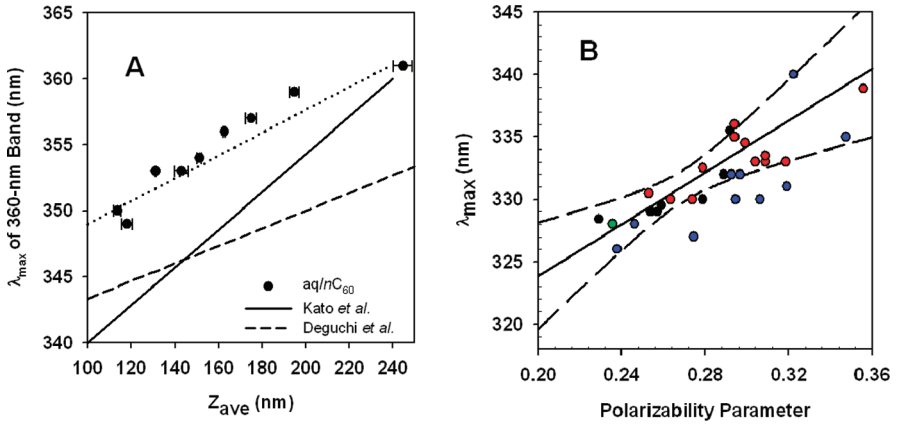

Figure 4. (A) λ_{max} as a function of Z_{ave} and (B) polarizability parameter vs λ_{max} (black dots are from Bensasson et al.;[2] red dots are from Gallagher et al.;[8] the green dot is from Renge;[5] blue dots are from Gun'kin and Loginova.[34] These data are summarized in Table S1 in the SI; the solid line represents a linear fit of all data and the dashed lines represent the 95% confidence interval).

concentration range aggregation of C_{60} becomes increasingly sterically hindered and C_{60} becomes more finely dispersed. If we consider the linear trends obtained from the regression of $\lambda_{max}(360)$ and Z_{ave} (Figure 4A) and extrapolate to Z_{ave} = 0.7 nm (e.g., the diameter of one C_{60} molecule), the calculated $\lambda_{max}(360)$ value should represent the position of the 360 nm absorption band for a "hypothetical" aqueous molecular C_{60} solution, wherein C_{60} is dispersed in water as individual molecules. The three experimentally predicted values, obtained via this calculation, increase in the order of Kato (326 nm) < Deguchi (337 nm) ≈ our study (340 nm). The differences among these values presumably reflect the different nC_{60} preparation procedures and isolation procedures employed. Kato et al. produced their nC_{60} via solvent exchange with tetrahydrofuran (THF/nC_{60}). This protocol involves the initial dissolution of fullerene C_{60} in THF, mixing the solution with water, and then removing the THF by sonication.[23] In this synthesis approach, THF residues (e.g., THF[23,25,28] or its derivatives[23,38]) potentially surround C_{60} and therefore may prevent it from fully interacting with water. As a result, the calculated $\lambda_{max}(360)$ value for THF/nC_{60} may actually reflect interactions between C_{60} molecules and residual organic solvent rather than just C_{60} and water. This hypothesis is supported by the fact that the calculated $\lambda_{max}(360)$ of the "aqueous molecular C_{60} solution" determined for THF/nC_{60} (= 326 nm) is close to that of a C_{60}−THF solution (= 328 nm) as reported by Gun'kin and Longinova.[34] SDS/SON/nC_{60}, which was obtained by ultrasonicating fullerene C_{60} powder in 40 mM sodium dedecylfulfate (SDS) in the Deguchi et al. study, has a $\lambda_{max}(360)$ similar to aq/nC_{60} despite the fact that the interactions between a C_{60} molecule and water are expected to be altered by the presence of the surfactant.

Compared with THF/nC_{60} and SDS/SON/nC_{60}, there were no other constituents in the aq/nC_{60} suspensions except for C_{60} and water. Therefore, the aq/nC_{60} nanoparticles are surrounded by water and the only possible interaction at the water−solid interface is the C_{60}−water interaction. The value for λ_{max} (= 340 nm) obtained by extrapolation of the trends in Figure 4A is much larger than that predicted based solely on the polarizability parameter (= 325 ± 6.4 nm). This red shift in the predicted band location is indicative of a different type of interaction between water and C_{60} relative to those between C_{60} and apolar organic solvents.[39] In aromatic solvents, strong $\pi-\pi$ interactions increase C_{60} solubility and are responsible for a red shift in this band.[6] Similarly, in polar solvents (e.g., THF), charge-transfer interactions[25] result in a red shift. We attribute the predicted red shift for C_{60}−water solutions to charge-transfer interactions. Recently it was found that hydration of C_{60} results in surface hydroxylation and a fullerenol-like nC_{60} surface.[32] In addition, Wi et al.[39] recently reported the presence of ordered water molecules at the aq/nC_{60} surface. Each of these occurrences would enhance the attraction between polar water molecules and the C_{60} surface and as such would result in a red-shift.

Changes in the 400−600 nm Region. In Figure 2B and Figure S2C, the normalized spectra of aq/nC_{60} in the 400−600 nm region are presented. The relative intensity of this broad continuous absorption band decreases during the extended mixing period concomitant with the observed decrease in the average particle size (Figure S1). In addition, the shape of this absorption band changes over time with its λ_{max} shifting from 540 to 460 nm.

The origin of this continuous band in the aq/nC_{60} spectrum has been under debate for some time. Some studies attribute it to the formation of weak donor−acceptor complexes of C_{60} with water or other aqueous constituents that have the ability to serve as electron donors.[28,34] A second hypothesis suggests that this band arises due to the presence of solid and crystalline C_{60},[14,23,25] in which close electronic interactions among adjacent C_{60} molecules produce the measured absorbance.[40]

In the present study, the relative intensity of this band was used to determine its origin. Bensasson et al.[2] have shown that aggregation of C_{60} in organic solvents has a strong effect on the oscillator strength of the intense 6-$^1T_{1u}$-1^1A_g (≈ 275 nm) allowed transition, but a lesser effect on the weaker 3-$^1T_{1u}$-1^1A_g (≈ 360 nm) transition. This result indicates that the 360-nm absorption band is less sensitive to C_{60}−C_{60} interactions (i.e., nanoparticle formation) than the 275-nm band. Given this fact, we calculated the ratio of the absorbance at 450 nm to the absorbance at 360 nm to determine the relative intensity of the broad absorption band from 400 to 600 nm.

Electron donor−acceptor interactions should occur primarily at the surface of nC_{60}. As a result, an absorption band produced in response to donor−acceptor complex formation should exhibit an increase in relative intensity as the fraction of C_{60} molecules at the nanoparticle surface (f_s) increases. A simple calculation to estimate f_s for a spherical nC_{60} nanoparticle can be readily derived:

$$n_{total} = \frac{4\pi}{3}\left(\frac{Z_{ave}}{2}\right)^3 \frac{4}{l^3} \quad (5)$$

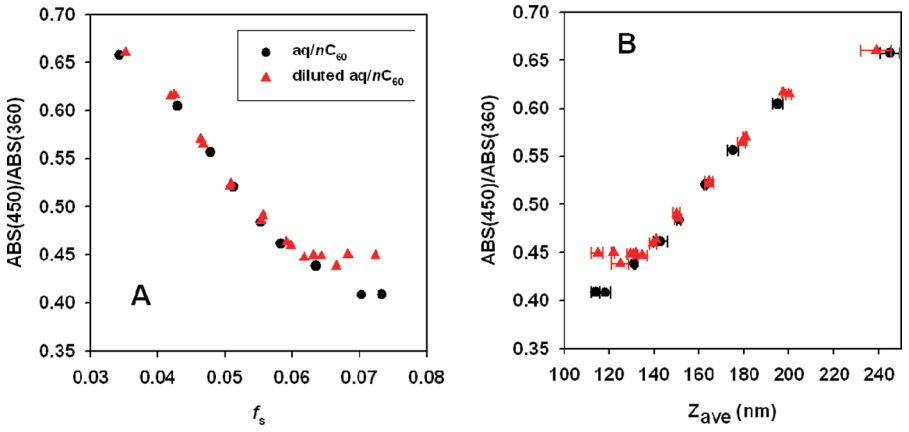

Figure 5. Relative intensity of 400−600 absorption band as a function of (A) fraction of surface C_{60} molecules and (B) Z_{ave}. The Z_{ave} value represented in this figure is the average of three measurements and the error bar represents the standard deviation of three measurements. To account for concentration-dependent variations in the baseline, the calculated ratio was normalized to the flat, but concentration-dependent, baseline by subtracting the measured Abs(800) from each Abs(450) and Abs(360) measurement.

$$n_{surface} = n_{total} - \frac{4\pi}{3}\left(\frac{Z_{ave}}{2} - l\right)^3 \frac{4}{l^3} \quad (6)$$

$$f_s = \frac{n_{surface}}{n_{total}} = 1 - \left(1 - \frac{2l}{Z_{ave}}\right)^3 \quad (7)$$

where n_{total} is the total number of C_{60} molecules contained in a spherical nC_{60} nanoparticle of diameter Z_{ave} (nm); l is the lattice constant of an aq/nC_{60} particle (= 1.417 nm[41]) with *fcc* crystallinity; and $n_{surface}$ is the number of C_{60} molecules present in the surface layer of the spherical particle. Figure 5A shows that the relative intensity of the 400−600 nm absorption band decreases with f_s. A recent paper[42] provided another method to estimate f_s. Although this method could increase the accuracy of our estimates since it takes the fractal dimension of the agglomerates into consideration, we were unable to use it herein because we do not know the fractal dimension of our aq/nC_{60}. Regardless of which method to estimate f_s is used, however, f_s is expected to be inversely correlated with Z_{ave} and the trend of an increase in relative intensity with an increase in f_s remains. This finding indicates that donor−acceptor complex formation is not the origin of this band.

If the interactions among C_{60} molecules in a crystalline nC_{60} particle are the origin of the 400−600 nm absorption band, the relative intensity should increase with an increase in Z_{ave}.[19] Data from our centrifugation experiments (Figure 5B) fit this predicted trend well. This calculation thus supports, but does not prove, the hypothesis that the close association between individual C_{60} molecules in aq/nC_{60} is responsible for the 400−600 nm continuous absorption band. Importantly, according to Figure 5B, the ABS(450)/ABS(360) ratio increases proportionally with the average particle size for Z_{ave} values larger than 120 nm. Calculation of this ratio can thus be made to estimate the average size of nC_{60} suspensions that meet this criterion. This prediction should be more reliable than that obtained from the relationship between $\lambda_{max}(360)$ and Z_{ave} (i.e., Figure 4) since $\lambda_{max}(360)$ is strongly affected by solution chemistry. It has previously been established that absorbance ratios are generally more robust and less subject to variation.[2]

Environmental Implications. Aq/nC_{60} produced via extended mixing is arguably a better approximation of the nanoparticles that will form when C_{60} is released to the environment than nC_{60} produced via methodologies involving the use of organic solvents or intense sonication conditions. During its formation, aq/nC_{60} exhibits progressive changes in its UV−vis spectra. The changes in the 240−290 nm region imply that the interaction between C_{60} and water is a temporal process and that the affinity of C_{60} with water varies over time. The rate at which this process occurs in natural waters could be either diminished or accelerated depending upon the solution composition. In any case, however, the progressive nature of the reaction should be considered to truly evaluate the reactivity and fate of C_{60} in aqueous environments.

As documented herein, the nC_{60} particle size is an important factor that dictates its UV−vis spectroscopic properties. The relative intensity of the continuous absorption band in the 400−600 nm region and the position of absorption maximum of the 360 nm band are proportional to the Z_{ave} of nC_{60}. With continued development, these relationships have the potential to be used to predict particle sizes in the absence of DLS data. However, $\lambda_{max}(360)$ is affected by the presence of other constituents in solution, indicating that size prediction by $\lambda_{max}(360)$ should be carefully conducted with continual awareness of the sample preparation methodology. Extrapolation of the relationship between $\lambda_{max}(360)$ and Z_{ave} reveals that the strong interaction between C_{60} and water is different from the interactions between C_{60} and organic solvents.

■ ASSOCIATED CONTENT

Supporting Information. Surface charge and average particle size of aq/nC_{60} as a function of stirring time, normalized spectra of aq/nC_{60} in different wavelength ranges, surface charge and average particle size of centrifuged aq/nC_{60}, UV−vis spectra of centrifuged aq/nC_{60}, λ_{max} changes of two major absorption bands for centrifuged aq/nC_{60} (stock suspensions and diluted stock suspensions), and λ_{max} of C_{60}-organic solutions and the refractive index of these organic solvents. This material is available free of charge via the Internet at http://pubs.acs.org.

■ AUTHOR INFORMATION

Corresponding Author

*E-mail: pvikes@vt.edu; phone: 540-231-3568; fax: 540-231-7916.

■ ACKNOWLEDGMENT

This material is based upon work supported by the National Science Foundation (NSF) and the Environmental Protection Agency (EPA) under NSF Cooperative Agreement EF-0830093, Center for the Environmental Implications of NanoTechnology (CEINT). Any opinions, findings, conclusions or recommendations expressed in this material are those of the author(s) and do not necessarily reflect the views of the NSF or the EPA. This work has not been subjected to EPA review and no official endorsement should be inferred. Additional funding was provided by the National Science Foundation (BES-0537117). Additional support from ICTAS for X.C. is gratefully acknowledged.

■ REFERENCES

(1) Leach, S.; Vervloet, M.; Despres, A.; Breheret, E.; Hare, J. P.; Dennis, T. J.; Kroto, H. W.; Taylor, R.; Walton, D. R. M. Electronic-spectra and transition of the fullerene C_{60}. *Chem. Phys.* **1992**, *160* (3), 451–466.

(2) Bensasson, R. V.; Bienvenue, E.; Dellinger, M.; Leach, S.; Seta, P. C_{60} in model biological -systems - A visible-UV absorption absorption study of solvent-dependent parameters and solute aggregation. *J. Phys. Chem.* **1994**, *98* (13), 3492–3500.

(3) Rao, C. N. R., *Ultra-violet and Visible Spectroscopy*; Butterworth & Co Ltd: Boston, 1975.

(4) Sassara, A.; Zerza, G.; Chergui, M.; Leach, S. Absorption wavelengths and bandwidths for interstellar searches of C_{60} in the 2400−4100 angstrom region. *Astrophys. J. Suppl. Ser.* **2001**, *135* (2), 263–273.

(5) Renge, I. Solvent effects on the absorption maxima of fullerene C_{60} and C_{70}. *J. Phys. Chem.* **1995**, *99* (43), 15955–15962.

(6) Sivaraman, N.; Dhamodaran, R.; Kaliappan, I.; Srinivasan, T. G.; Rao, P. R. V.; Mathews, C. K. Solubility of C_{60} in organic-solvents. *J. Org. Chem.* **1992**, *57* (22), 6077–6079.

(7) Heymann, D. Solubility of C-60 in alcohols and alkanes. *Carbon* **1996**, *34* (5), 627–631.

(8) Gallagher, S. H.; Armstrong, R. S.; Lay, P. A.; Reed, C. A. Solvent effects on the electronic-spectrum of C_{60}. *J. Phys. Chem.* **1995**, *99* (16), 5817–5825.

(9) Scrivens, W. A.; Tour, J. M.; Creek, K. E.; Pirisi, L. Synthesis of C-14-labeled C_{60}, its suspension in water, and its uptake by human keratinocytes. *J. Am. Chem. Soc.* **1994**, *116* (10), 4517–4518.

(10) Andrievsky, G. V.; Kosevich, M. V.; Vovk, O. M.; Shelkovsky, V. S.; Vashchenko, L. A. On the production of an aqueous colloidal solution of fullerenes. *J. Chem. Soc., Chem. Commun.* **1995**, *12*, 1281–1282.

(11) Deguchi, S.; Alargova, R. G.; Tsujii, K. Stable dispersions of fullerenes, C_{60} and C_{70}, in water. Preparation and characterization. *Langmuir* **2001**, *17* (19), 6013–6017.

(12) Duncan, L. K.; Jinschek, J. R.; Vikesland, P. J. C_{60} colloid formation in aqueous systems: Effects of preparation method on size, structure, and surface, charge. *Environ. Sci. Technol.* **2008**, *42* (1), 173–178.

(13) Brant, J.; Lecoanet, H.; Hotze, M.; Wiesner, M. Comparison of electrokinetic properties of colloidal fullerenes (nC_{60}) formed using two procedures. *Environ. Sci. Technol.* **2005**, *39* (17), 6343–6351.

(14) Scharff, P.; Carta-Abelmann, L.; Siegmund, C.; Matyshevska, O. P.; Prylutska, S. V.; Koval, T. V.; Golub, A. A.; Yashchuk, V. M.; Kushnir, K. M.; Prylutskyy, Y. I. Effect of X-ray and UV irradiation of the C_{60} fullerene aqueous solution on biological samples. *Carbon* **2004**, *42* (5−6), 1199–1201.

(15) Xie, B.; Xu, Z. H.; Guo, W. H.; Li, Q. L. Impact of natural organic matter on the physicochemical properties of aqueous C_{60} nanoparticles. *Environ. Sci. Technol.* **2008**, *42* (8), 2853–2859.

(16) Isaacson, C. W.; Bouchard, D. C. Effects of humic acid and sunlight on the generation and aggregation state of aqu/C_{60} nanoparticles. *Environ. Sci. Technol.* **2010**, *44* (23), 8971–8976.

(17) Li, Q. L.; Xie, B.; Hwang, Y. S.; Xu, Y. J. Kinetics of C_{60} fullerene dispersion in water enhanced by natural organic matter and sunlight. *Environ. Sci. Technol.* **2009**, *43* (10), 3574–3579.

(18) Kilpatrick, P. K.; Miller, W. G.; Talmon, Y. Staining and drying-induced artifacts in electron-microscopy of surfactant dispersions. 2. Change in phase-behavior produced by variation in pH modifiers, stain, and concentration. *J. Colloid Interface Sci.* **1985**, *107* (1), 146–158.

(19) Kato, H.; Nakamura, A.; Takahashi, K.; Kinugasa, S. Size effect on UV-Vis absorption properties of colloidal C_{60} particles in water. *Phys. Chem. Chem. Phys.* **2009**, *11* (25), 4946–4948.

(20) Deguchi, S.; Mukai, S.; Yamazaki, T.; Tsudome, M.; Horikoshi, K. Nanoparticles of fullerene C_{60} from engineering of antiquity. *J. Phys. Chem. C* **2010**, *114* (2), 849–856.

(21) Chang, X.; Vikesland, P. J. Effects of carboxylic acids on nC(60) aggregate formation. *Environ. Pollut.* **2009**, *157* (4), 1072–1080.

(22) Cheng, X. K.; Kan, A. T.; Tomson, M. B. Naphthalene adsorption and desorption from aqueous C_{60} fullerene. *J. Chem. Eng. Data* **2004**, *49* (3), 675–683.

(23) Brant, J. A.; Labille, J.; Bottero, J. Y.; Wiesner, M. R. Characterizing the impact of preparation method on fullerene cluster structure and chemistry. *Langmuir* **2006**, *22* (8), 3878–3885.

(24) Belousova, I. M.; Belousov, V. P.; Kiselev, V. M.; Murav'eva, T. D.; Kislyakov, I. M.; Sirotkin, A. K.; Starodubtsev, A. M.; Kris'ko, T. K.; Bagrov, I. V.; Ermakov, A. V. Structural and optical properties of solid-phase singlet oxygen photosensitizers based on fullerene aqueous suspensions. *Opt. Spectrosc.* **2008**, *105* (5), 711–719.

(25) Fortner, J. D.; Lyon, D. Y.; Sayes, C. M.; Boyd, A. M.; Falkner, J. C.; Hotze, E. M.; Alemany, L. B.; Tao, Y. J.; Guo, W.; Ausman, K. D.; Colvin, V. L.; Hughes, J. B. C_{60} in water: Nanocrystal formation and microbial response. *Environ. Sci. Technol.* **2005**, *39* (11), 4307–4316.

(26) Eastoe, J.; Crooks, E. R.; Beeby, A.; Heenan, R. K. Structure and photophysics in C_{60}-micellar solutions. *Chem. Phys. Lett.* **1995**, *245* (6), 571–577.

(27) Achiba, Y.; Nakagawa, T.; Matsui, Y.; Suzuki, S.; Shiromaru, H.; Yamauchi, K.; Nishiyama, K.; Kainosho, M.; Hoshi, H.; Maruyama, Y.; Mitani, T. Visible, UV, and VUV absorption-spectra of C_{60} thin-films grown by the molecular-beam epitaxy (MBE) technique. *Chem. Lett.* **1991**, *7*, 1233–1236.

(28) Andrievsky, G. V.; Klochkov, V. K.; Bordyuh, A. B.; Dovbeshko, G. I. Comparative analysis of two aqueous-colloidal solutions of C_{60} fullerene with help of FTIR reflectance and UV-Vis spectroscopy. *Chem. Phys. Lett.* **2002**, *364* (1−2), 8–17.

(29) Chen, Z.; Westerhoff, P.; Herckes, P. Quantification of C_{60} fullerene concentrations in water. *Environ. Toxicol. Chem.* **2008**, *27* (9), 1852–1859.

(30) Ma, X.; Wigington, B.; Bouchard, D. Fullerene C_{60}: Surface energy and interfacial interactions in aqueous systems. *Langmuir* **2010**, *26* (14), 11886–11893.

(31) Isaacson, C.; Zhang, W.; Powell, T.; Ma, X.; Bouchard, D. Temporal changes in aqu/C_{60} physical-chemical, deposition, and transport characteristics in aqueous systems. *Environ. Sci. Technol.* **2011**, *45* (12), 5170–5177.

(32) Labille, J.; Masion, A.; Ziarelli, F.; Rose, J.; Brant, J.; Villieras, F.; Pelletier, M.; Borschneck, D.; Wiesner, M. R.; Bottero, J. Y. Hydration and dispersion of C_{60} in aqueous systems: The nature of water-fullerene interactions. *Langmuir* **2009**, *25* (19), 11232–11235.

(33) Hassellov, M.; Readman, J. W.; Ranville, J. F.; Tiede, K. Nanoparticle analysis and characterization methodologies in environmental risk assessment of engineered nanoparticles. *Ecotoxicology* **2008**, *17* (5), 344–361.

(34) Gun'kin, I. F.; Loginova, N. Y. Effect of nature of organic solvent on the absorption spectrum of C_{60} fullerene. *Russ. J. Gen. Chem.* **2006**, *76* (12), 1911–1913.

(35) Reichardt, C. *Solvents and Solvent Effects in Organic Chemistry*, 2nd ed.; VCH Verlagsgesellaschaft: Weinheim, 1988.

(36) Seshadri, R.; Rao, C. N. R.; Pal, H.; Mukherjee, T.; Mittal, J. P. Interaction of C_{60} and C_{70} with aromatic amines in the ground and

excited states. Evindence for fullerene--benzene interaction in the ground state. *Chem. Phys. Lett.* **1993**, *205* (4−5), 395–398.

(37) Lee, J.; Kim, J. H. Effect of encapsulating agents on dispersion status and photochemical reactivity of C_{60} in the aqueous phase. *Environ. Sci. Technol.* **2008**, *42* (5), 1552–1557.

(38) Zhang, B.; Cho, M.; Fortner, J. D.; Lee, J.; Huang, C. H.; Hughes, J. B.; Kim, J. H. Delineating oxidative processes of aqueous C_{60} preparations: Role of THF peroxide. *Environ. Sci. Technol.* **2009**, *43* (1), 108–113.

(39) Wi, S.; Spano, J.; Ducker, W. A. Hindered rotation of water near C_{60}. *J. Phys. Chem. C* **2010**, *114* (35), 14986–14991.

(40) Hungerbuhler, H.; Guldi, D. M.; Asmus, K. D. Incorporation of C_{60} into artificial lipid-membranes. *J. Am. Chem. Soc.* **1993**, *115* (8), 3386–3387.

(41) Heiney, P. A.; Fischer, J. E.; McGhie, A. R.; Romanow, W. J.; Denenstein, A. M.; McCauley, J. P.; Smith, A. B.; Cox, D. E. Orientational ordering transition in solid C_{60}. *Phys. Rev. Lett.* **1991**, *66* (22), 2911–2914.

(42) Hotze, E. M.; Bottero, J. Y.; Wiesner, M. R. Theoretical framework for nanoparticle reactivity as a function of aggregation state. *Langmuir* **2010**, *26* (13), 11170–11175.